

Article

The Influence of Geometric Parameters of Pump Installation on the Hydraulic Performance of a Prefabricated Pumping Station

Bowen Zhang ¹, Li Cheng ^{1,*}, Chunlei Xu ² and Mo Wang ³

¹ College of Hydraulic Science and Engineering, Yangzhou University, Yangzhou 225009, China; DX120190073@yzu.edu.cn

² Key Water Conservancy Project Management Office, Wuxi 214000, China; xcl69@163.com

³ Anhui Branch of Hainan Water Resources and Hydropower Survey and Design Institute, Hefei 225000, China; wangmo2021@hotmail.com

* Correspondence: chengli@yzu.edu.cn

Abstract: A prefabricated pumping station is a new type of pumping station that plays an important role in the construction of sponge cities in developing countries. It solves the problem of urban water-logging and makes great contributions to the sustainable development of water resources. In order to research the influence of different installation positions of pumps on the internal hydraulic performance of a prefabricated pumping station, based on ANSYS software, the computational fluid dynamics (CFD) numerical simulation method was used to analyze the internal flow state of the prefabricated pump station. In this research, the optimal geometric parameters of pump installation in a prefabricated pumping station are given. The results show that when the distance between the connecting line of two pumps and the center of the sump is $L = 0.2 R$, the distance between the two pumps is $S = 0.6 R$, and the suspension height of the two pumps is $H = 0.6 D$, the internal flow pattern of the prefabricated pump station is better. (R is the cross-sectional radius of the sump and D is the diameter of the nozzle of the pump horn.) These research results have certain guiding significance for improvement of the hydraulic performance and operation efficiency of prefabricated pump stations. They also provide a theoretical basis for parameter selection for prefabricated pumping stations.

Keywords: prefabricated pumping station; hydraulic performance; geometric parameter; installation position; numerical simulation



Citation: Zhang, B.; Cheng, L.; Xu, C.; Wang, M. The Influence of Geometric Parameters of Pump Installation on the Hydraulic Performance of a Prefabricated Pumping Station. *Energies* **2021**, *14*, 1039. <https://doi.org/10.3390/en14041039>

Academic Editor: Riccardo Amirante

Received: 5 January 2021

Accepted: 12 February 2021

Published: 16 February 2021

Publisher's Note: MDPI stays neutral with regard to jurisdictional claims in published maps and institutional affiliations.



Copyright: © 2021 by the authors. Licensee MDPI, Basel, Switzerland. This article is an open access article distributed under the terms and conditions of the Creative Commons Attribution (CC BY) license (<https://creativecommons.org/licenses/by/4.0/>).

1. Introduction

With the acceleration of the urbanization process in developing countries, as well as the construction of various infrastructure, more and more wastewater needs to be lifted and transported by pumping stations. In the sewage treatment system, the sewage treatment plant is the “kidney”, the pipelines are the “blood vessels”, and the pumping stations all over the city are like “hearts”, which continuously and stably transport the collected sewage to the treatment center after pretreatment. Traditional concrete pumping stations have the disadvantages of large area, difficult planning, long construction period, and high cost. When the concrete pump station is put into use, due to the low level of integration and automation, it needs to be manually kept on duty and maintained.

A prefabricated pumping station is a kind of pumping station which integrates the storage tank, pump, pipeline, control system, and ventilation system. The pre-installation and testing are completed before delivery [1]. The cylinder of the prefabricated pumping station is made of glass-fiber-reinforced plastics (GFRP) or high-density polyethylene (HDPE). It has the characteristics of light weight, high strength, and strong corrosion resistance. The prefabricated pumping station is equipped with two submersible sewage pumps, automatic coupling device, guide rod, lifting chain, inlet pipe, check valve, gate valve, and outlet pipe [2] (Figure 1). With the construction of sponge cities in developing countries, prefabricated pumping stations have gradually become the first choice for

municipal drainage systems. As a substitute for small and medium-sized concrete pumping stations, prefabricated pumping stations contribute to the treatment of urban water-logging, which is of great significance to the sustainable development of water resources.

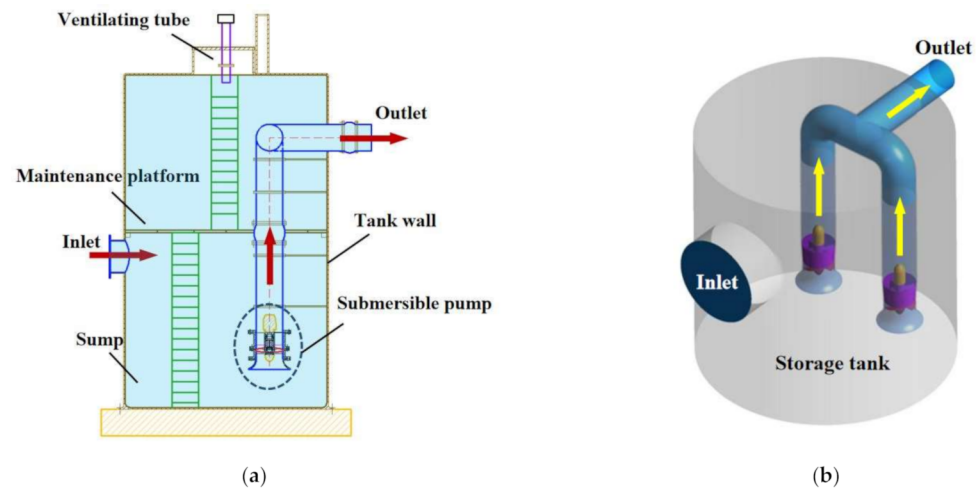


Figure 1. A typical prefabricated pumping station: (a) Schematic diagram of main components; (b) Three-dimensional diagram.

The working environment of the submersible sewage pump in a prefabricated pumping station is similar to that of the pump in a traditional pump station with closed intake sump [3–5]. Both of them have no free water surface, and the pump directly absorbs water without passing through the inlet pipe or channel. In this respect, domestic and foreign scholars have made great achievements in experimental research and optimization design [6,7]. Charles [8] put forward that the average velocity in the pool should be kept at about 0.3 m/s when the width of the inlet pool is designed. Iversen [9] gave the range of submergence depth of a high-specific-speed intake tank. Following from a tremendous number of experiments, Japan Association of Agricultural Engineering Enterprises [10] gave reference value ranges for the important dimensions of pump suspension height, submergence depth, back wall distance, pool width, and pool length. Fraser [11] studied the vortex problem in the intake pool of a pumping station and put forward a solution. Nsar [12] analyzed the flow pattern in a pump inlet tank with and without tangential reflux at the inlet of the rectangular inlet tank.

So far, many scholars have also conducted relevant research on prefabricated pumping stations. Liu Q. et al. [13] used computational fluid dynamics (CFD) methods to optimize the geometric parameters of storage tanks in prefabricated pumping stations. The relationship between tank bottom diameter and tank height was studied, and the basic mechanism of sediment deposition in prefabricated pumping stations was expounded. Based on the discrete solid–liquid two-phase flow model (DPM) and MATLAB image processing technology, Kang W. et al. [14] analyzed the settlement characteristics of a prefabricated pumping station under the action of a single pump and double pumps and measured the movement track of sediment particles at the bottom of the pump station. Qing L. et al. [15] revealed the flow characteristics of water and sediment in the prefabricated pumping station and optimized the geometric parameters of the water tank to reduce sand deposition. The results show that the risk of sediment deposition is high at the bottom side near the inlet of the pumping station, and the geometry of the pump bottom and the suction of the pump inlet are conducive to sand deposition. Due to the lack of suitable dispatching facilities in the drilling area of southern Mexico, Medina, A P [16] proposed a design scheme of a closed circulating prefabricated pumping station. Hu et al. [17] optimized the effective volume of the prefabricated pumping station through calculation. In order to reduce the volume of the integrated prefabricated pumping station, the minimum start-up and stop time interval of the pump was derived. Hu [18] proposed a self-cleaning solution to solve the problem of

residual debris and deposition inside prefabricated pumping stations. Cheng Li et al. [19] invented a self-cleaning measure for the bottom of prefabricated pumping stations. An arc rib embedded in the bottom of the tank surface was used to realize self-cleaning.

Previous studies on integrated pumping stations focus on the submersible centrifugal pump and its specific applications in engineering. However, there are few studies on the influence of the geometric parameters of a submersible axial-flow pump on prefabricated pumping stations. Based on computational fluid dynamics (CFD), the influence of the geometric parameters of the submersible axial-flow pump installation position on the internal hydraulic performance of a prefabricated pump station is studied and analyzed herein. The optimal geometric parameters of pump installation are thus recommended. This can improve the pump station's internal flow pattern and improve its operation efficiency. At the same time, the research results also provide a theoretical basis for parameter selection for prefabricated pumping stations.

2. Research Model and Numerical Calculation

2.1. Hydrodynamic Equations

The Navier–Stokes (N-S) equation is a motion equation describing the momentum conservation of viscous and incompressible fluid. The N-S equation is composed of three equations of fluid flow: the mass conservation equation, momentum conservation equation, and energy conservation equation. These correspond to the three conservation laws, namely, the law of conservation of energy, the law of conservation of momentum, and the law of conservation of mass. The expression of the N-S equation in the rectangular coordinate system is [20,21]

$$\frac{\partial u_i}{\partial x_i} = 0, \quad (1)$$

$$\frac{\partial}{\partial t}(\rho u_i) + \frac{\partial}{\partial x_j}(\rho u_i u_j) = -\frac{\partial p}{\partial x_i} + \frac{\partial \tau_{ij}}{\partial x_i} + \rho g_i + F_i, \quad (2)$$

where u_i is the three-dimensional velocity component, x_i is the three-dimensional coordinate component, p is the pressure, ρg_i is the gravity term, and F_i is the external source term. τ_{ij} is the stress tensor, its expression is as follows:

$$\tau_{ij} = \left[\mu \left(\frac{\partial u_i}{\partial x_j} + \frac{\partial u_j}{\partial x_i} \right) \right] - \frac{2}{3} \mu \delta_{ij} \frac{\partial u_i}{\partial x_j}, \quad (3)$$

where μ_{ij} is the dynamic viscosity and δ_{ij} is the Kronecker delta sign (when $i = j$, $\delta_{ij} = 1$; when $i \neq j$, $\delta_{ij} = 0$).

If the influence of gravity is neglected, the momentum equation can be simplified to

$$\frac{\partial}{\partial t}(\rho u_i) + \frac{\partial}{\partial x_j}(\rho u_i u_j) = -\frac{\partial p}{\partial x_i} + \frac{\partial}{\partial x_j} \left[\mu \left(\frac{\partial u_i}{\partial x_j} + \frac{\partial u_j}{\partial x_i} \right) \right] + F_i. \quad (4)$$

The Reynolds averaged N-S (RANS) equation is based on the time-averaged treatment of the transient N-S equation and supplemented with other equations reflecting the turbulence characteristics. The turbulence model theory based on the Reynolds averaged N-S equation has become the mainstream theory in the calculation of pump internal flow fields [22,23].

The time mean and fluctuating values of velocity and pressure are decomposed as follows:

$$u_i = \bar{u}_i + u'_i, \quad (5)$$

$$p = \bar{p} + p', \quad (6)$$

where u_i is the instantaneous velocity in direction i , \bar{u}_i is the average velocity in direction i , u'_i is the pulsating value of velocity in direction i , \bar{p} is the mean pressure, and p' is

the pulsating pressure. By substituting the above two equations into (1) and (4), the time-averaged N-S equation can be obtained.

Continuity equation:

$$\frac{\partial \bar{u}_i}{\partial x_i} = 0, \quad (7)$$

Momentum equation:

$$\frac{\partial}{\partial x_j} (\rho \bar{u}_i \bar{u}_j) = -\frac{\partial \bar{p}}{\partial x_i} + \frac{\partial}{\partial x_i} \left[\mu \left(\frac{\partial \bar{u}_i}{\partial x_j} + \frac{\partial \bar{u}_j}{\partial x_i} \right) - \rho \overline{u'_i u'_j} \right] + F_i. \quad (8)$$

Equations (7) and (8) are the mathematical expressions of the RANS equation. The internal flow of a prefabricated pumping station is unsteady viscous flow. Therefore, the RANS equation was used as the basic governing equation to describe the flow law.

In the process of numerical simulation, the meshing software ICEM CFD of ANSYS, the fluid analysis software ANSYS CFX, and the visualization post-processing software Tecplot were used.

ANSYS CFX is a mature commercial fluid computing software with the most advanced algorithm in the world, which adopts the full implicit algorithm. Its rich physical models and the perfection of preprocessing and post-processing give CFX excellent performance in terms of the accuracy, stability, speed, and flexibility of results [24–26]. It includes three parts: CFX-pre, CFX-solver, and CFX-post.

2.2. Physical Models

Figure 2 shows the structure of the prefabricated pumping station model. The numerical calculation area includes one collecting basin, one water inlet, two outlet pipes, and two symmetrical submersible axial-flow pumps. The pump includes an impeller, guide vane, and two submersible motors.

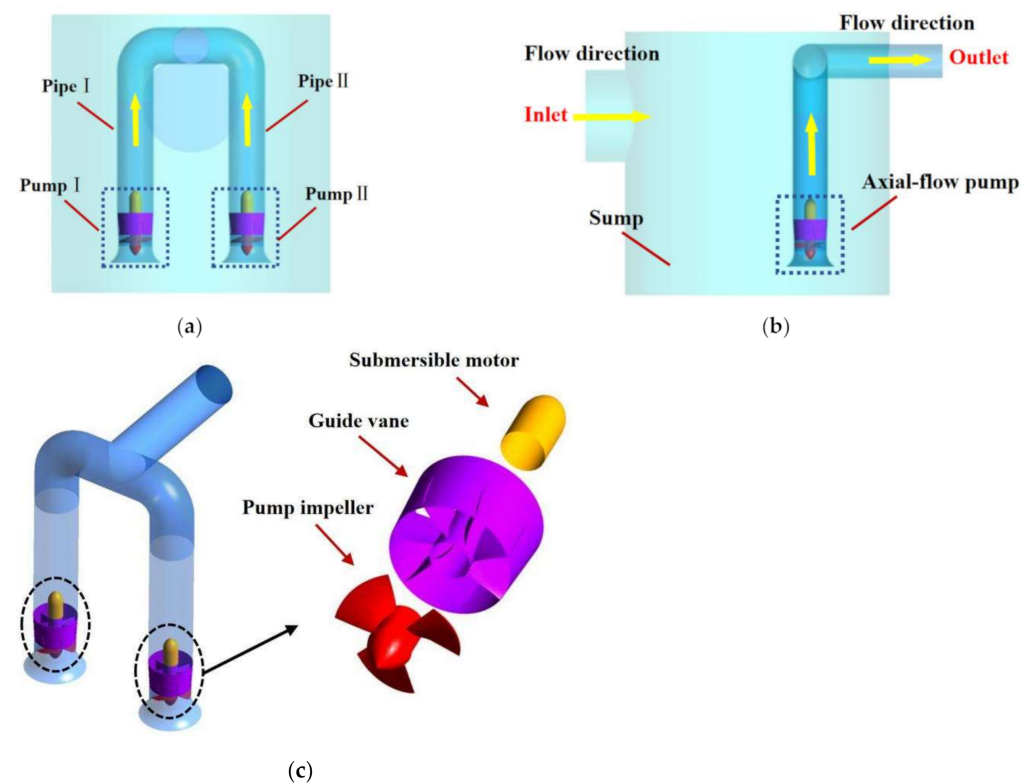


Figure 2. The structure of the prefabricated pumping station model. (a) Front view of the model; (b) Side view of the model; (c) Structure of the submersible axial-flow pump.

According to the relevant literature and the operation practice recommended by the manufacturer [27,28], the relationship between the effective volume of the storage tank and the flow rate of the prefabricated pumping station is $V = Q_b/4Z_{\max}$, where Q_b is the pump flow and Z_{\max} is the maximum number of starts and stops (10~30 times/hour). A Z_{\max} value of 15 times/hour was used to match the relationship between the effective volume and the flow rate of the pump. The water body of the tank was selected as a cylinder with diameter and height of 1 m in the research. The design flow of each single pump was 198 m³/hour. The impeller diameter of the pump was 120 mm, the number of blades was 3, and the speed was 2400 rev/min. The two pumps were run at the same time.

2.3. Mesh Generation and Grid Independence Examination

The grid was divided into blocks. The prefabricated pumping station was divided into a sump, two pairs of impellers and guide vanes, two trumpet pipes, and two outlet pipes. As shown in Figure 3a, the impeller and guide vane were meshed using ICFM CFD. As shown in Figure 3b, an unstructured tetrahedral mesh was used in the mesh of the workbench for the sump and pipeline.

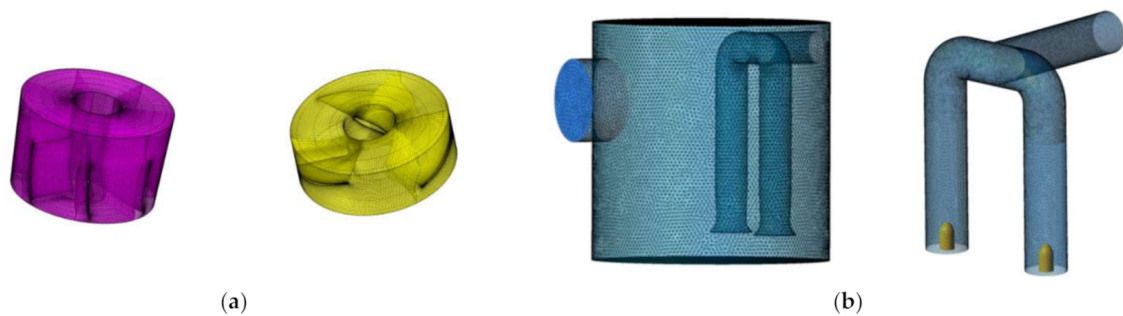


Figure 3. (a) Guide vane and impeller model grid; (b) Main body and pipe model grid of the sump.

We mainly checked the grid independence of the main part of the sump. The number of grid cells ranged between 900,000 and 1,300,000, and the efficiency of Pump I was used as the evaluation index. As can be seen from Table 1, the total number of grid cells used was 1,213,025.

Table 1. Grid cell quantity table.

Number	Number of Grid Cells	Efficiency of Pump I/%
1	907,745	47.25
2	1,018,955	49.68
3	1,108,631	50.43
4	1,213,025	50.51
5	1,301,298	50.49

2.4. Turbulence Model

The standard $k - \epsilon$ turbulence model was proposed by Launder B E and Spalding D B [29]. Based on the turbulent kinetic energy (k) equation, the turbulence dissipation rate (ϵ) equation is introduced into the turbulence model to form a two-equation model. The standard $k - \epsilon$ turbulence model is the most widely used turbulence model at present and is suitable for the fully developed turbulence calculation model with high Reynolds number [30]. We chose the standard $k - \epsilon$ turbulence model in this research. In the model, the turbulent dissipation rate ϵ is defined as

$$\epsilon = \frac{\mu}{\rho} \overline{\left(\frac{\partial u_i}{\partial x_k} \right) \left(\frac{\partial u_i}{\partial x_k} \right)} \quad (9)$$

The turbulent viscosity μ_t can be expressed as

$$\mu_t = \rho C_u \frac{k^2}{\varepsilon} \quad (10)$$

The equations of the turbulent kinetic energy k and turbulent energy dissipation ε are as follows:

$$\frac{\partial(\rho k)}{\partial t} + \frac{\partial(\rho k u_i)}{\partial x_i} = \frac{\partial}{\partial x_j} \left[\left(\mu + \frac{\mu_t}{\sigma_k} \right) \frac{\partial k}{\partial x_j} \right] + G_k - \rho \varepsilon \quad (11)$$

$$\frac{\partial(\rho \varepsilon)}{\partial t} + \frac{\partial(\rho \varepsilon u_i)}{\partial x_i} = \frac{\partial}{\partial x_j} \left[\left(\mu + \frac{\mu_t}{\sigma_\varepsilon} \right) \frac{\partial \varepsilon}{\partial x_j} \right] + C_{1\varepsilon} \rho \frac{\varepsilon}{k} G_k - C_{2\varepsilon} \rho \frac{\varepsilon^2}{k} \quad (12)$$

where G_k is the production term of turbulent kinetic energy k caused by buoyancy:

$$G_k = \mu_t \left(\frac{\partial u_i}{\partial x_j} + \frac{\partial u_j}{\partial x_i} \right) \frac{\partial u_i}{\partial x_j} \quad (13)$$

C_u , $C_{1\varepsilon}$, and $C_{2\varepsilon}$ are empirical constants, with $C_u = 0.09$, $C_{1\varepsilon} = 1.44$, and $C_{2\varepsilon} = 1.92$; σ_k and σ_ε are the Prandtl numbers corresponding to the turbulent kinetic energy k and dissipation rate ε , respectively, where $\sigma_k = 1.0$ and $\sigma_\varepsilon = 1.3$.

2.5. Boundary Conditions

The boundary conditions have a very important influence on the numerical calculation. The boundary conditions not only need to consider the influence of the turbulence model but also must be consistent with the physical model.

There are five boundary types in ANSYS CFX, which are inlet, outlet, opening, wall, and symmetry. The inlet boundary condition was set at the inlet section of the prefabricated pumping station. The outlet condition was set at the outlet section of the prefabricated pumping station. In this paper, the pump impeller is a rotating area, and the guide vane is a stationary area. The "Frozen rotor" was adopted for the type of dynamic and static interface. The specific conditions are shown in Table 2.

Table 2. Parameter settings for steady calculation.

Main Parameters	CFX Settings	Main Parameters	CFX Settings
Assumption condition	Steady, incompressible	Inlet condition	Mass flow
Turbulence model	Standard $k - \varepsilon$ turbulence model	Outlet condition	Static pressure
Near-wall function	Scalable wall function	Rotational speed	2400 rev/min
Wall	Non-slip	Impeller-guide vane interface	Frozen rotor

2.6. Geometric Parameters of Submersible Axial-Flow Pump Installation

The geometric parameters of pump installation include L (the distance between the connecting line of the two pumps and the center of the sump), S (the distance between the two pumps), and H (the suspension height of the two pumps).

As shown in Figure 4, section 1-1 is the longitudinal section of the two pumps perpendicular to L . Section 2-2 is the left longitudinal section at the center of Pump I and the right longitudinal section at the center of Pump II. The outlet pipe of Pump I is Pipe I, and that of Pump II; is Pipe II. Section 3-3 is the cross section between the sump bottom and the pump inlet. Section 4-4 is the cross section of the pump suction.

The geometric parameters of the pump installation position in the prefabricated pumping station were researched by a single-factor analysis method. Using a single-factor analysis method means that when one factor is analyzed, the other factors are fixed. This method can reasonably arrange research schemes, reduce the required number of studies, and quickly find the best scheme. Table 3 shows the parameter settings of the research

schemes. R is the cross-sectional radius of the sump and D is the diameter of the nozzle of the pump horn.

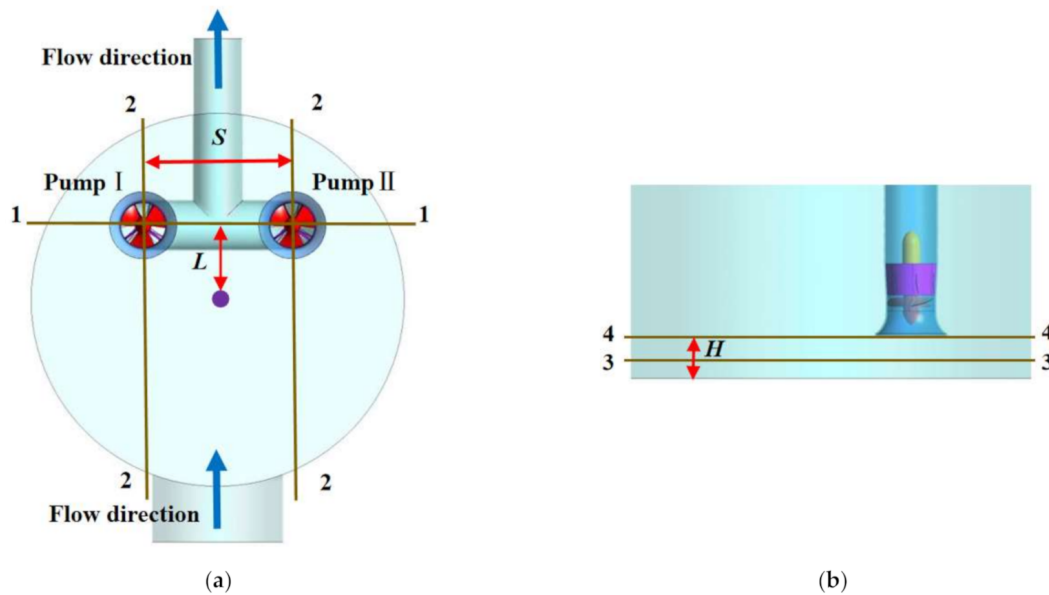


Figure 4. (a) Top view of the prefabricated pumping station model; (b) Front view of the prefabricated pumping station model.

Table 3. Single-factor geometric parameter schemes.

Scheme No.	L	S	H
1	$0.2 R$		
2	$0.4 R$	$0.6 R$	$0.6 D$
3	$0.6 R$		
4		$0.6 R$	
5		$0.8 R$	$0.6 D$
6		$1.0 R$	
7	$0.2 R$		$0.3 D$
8		$0.6 R$	$0.6 D$
9			$0.9 D$

3. Results

3.1. Influence of L on Hydraulic Performance

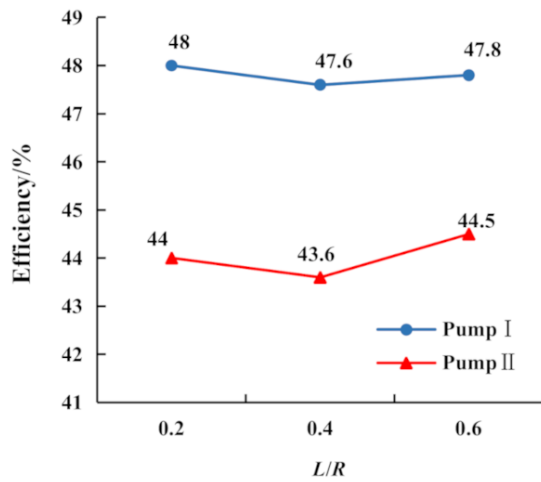
In order to explore the influence of different L values on the hydraulic performance of the prefabricated pumping station, we set the inlet mass flow to $Q = 55 \text{ kg/s}$, the suspension height of the pump to $H = 0.6 D$, and the distance between the two pumps to $S = 0.6 R$. The respective internal flow characteristics of prefabricated pumping stations with $L = 0.2 R$, $L = 0.4 R$, and $L = 0.6 R$ were then determined.

Figure 5a shows the curve of the influence of L on the efficiency of the two pumps. According to the curve, the influence of L on pump efficiency is small. The efficiency of Pump I was about 4% higher than that of Pump II due to the influence of asymmetric flow and pump suction in the sump.

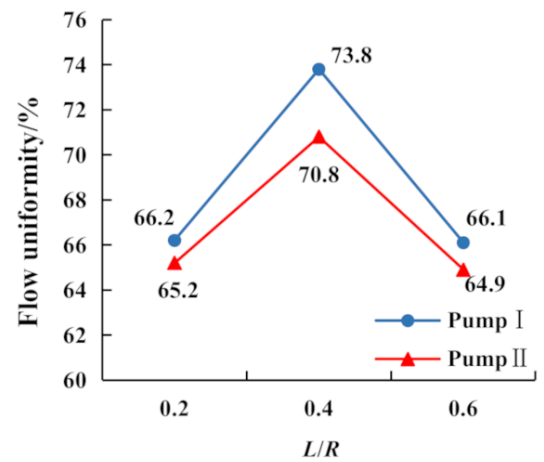
Figure 5b shows the variation curve of inlet velocity uniformity of the pump impeller chamber with L . According to the curve, when $L = 0.4 R$, the uniformity of the flow rate at the pump inlet was the highest. The uniformity of flow velocity at the inlet of Pump I was 1~4% higher than that of Pump II.

Figure 5c shows the curve of the weighted average angle of inlet velocity of the pump impeller chamber with L . It can be seen from the curve that the inlet velocity weighted average angle of the Pump I impeller chamber increased slowly with increasing L . However, the weighted average angle of the impeller chamber inlet velocity of Pump II showed a

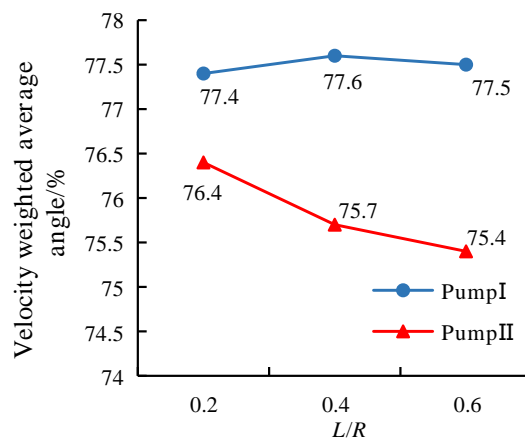
gradual downward trend with increasing L . The weighted average angle of inlet velocity of Pump I was higher than that of Pump II.



(a)



(b)



(c)

Figure 5. (a) The influence of L on the efficiency of the two pumps; (b) Variation of the inlet velocity uniformity of the pump impeller chamber with L ; (c) The weighted average angle of the inlet velocity of the pump impeller chamber with L .

Figures 6–8 show the streamline and velocity distribution nephograms of sections 2-2, 3-3, and 4-4, respectively, under different L values.

It can be seen from Figure 6 that when $L = 0.2 R$, the flow velocity at the water inlet was faster, and the water flow in the sump diffused up and down. When $L = 0.4 R$, the velocity at the inlet was faster and the vortex behind the outlet pipe decreased. However, there were small vortices in the upper position in front of the pipes. When $L = 0.6 R$, the vortex in the upper position behind the outlet pipe disappeared, and the vortex area in front of the outlet pipe increased obviously.

It can be seen from Figure 7; Figure 8 that vortices and high-speed zones appeared below the water inlet of the water pump. It can be seen from the velocity distribution diagram that the velocity in the central area of the sump was the highest, and the velocity gradually decreased with decreasing distance from the wall. When $L = 0.2 R$, the efficiency of the two pumps was the highest, and the weighted average angle of the impeller chamber inlet velocity was the largest.

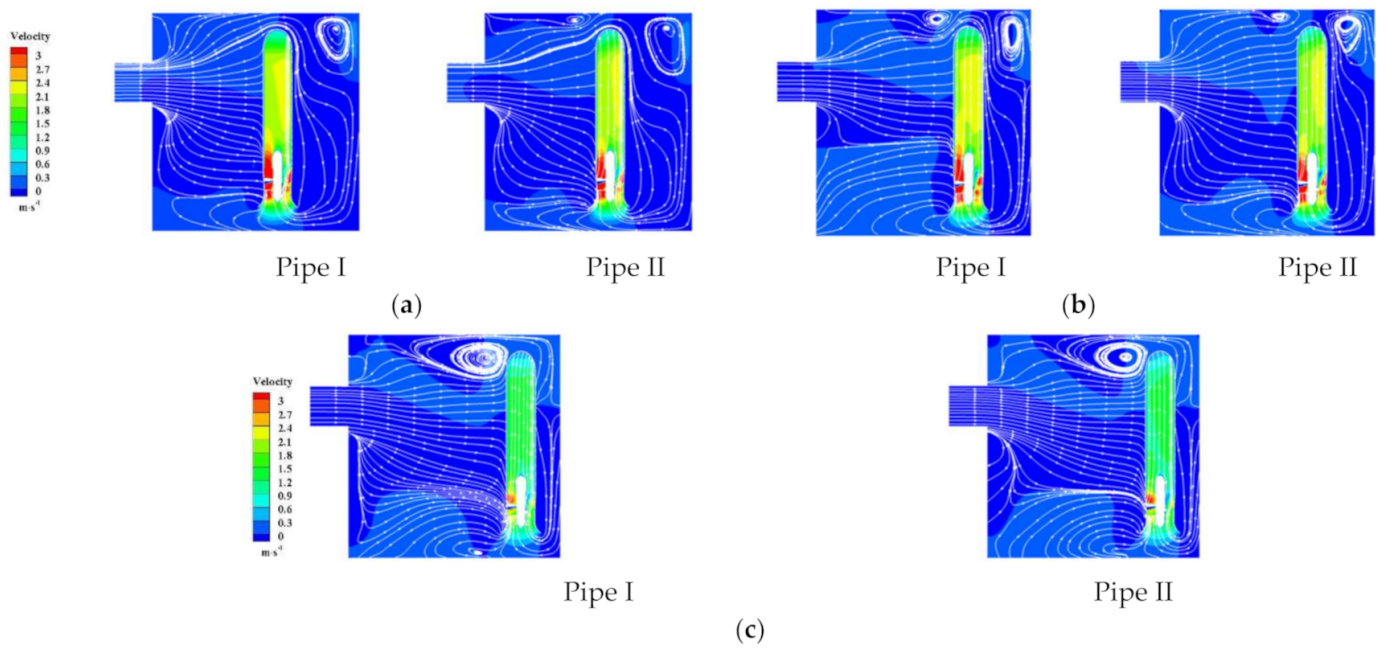


Figure 6. Streamline and velocity distribution nephogram of Section 2-2 under different L values: (a) $L = 0.2 R$; (b) $L = 0.4 R$; (c) $L = 0.6 R$.

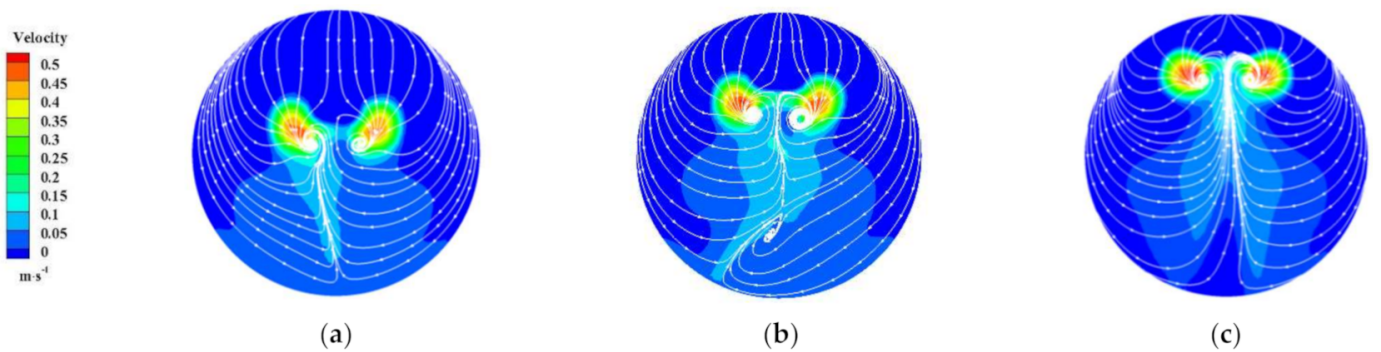


Figure 7. Streamline and velocity distribution nephogram of Section 3-3 under different L values: (a) $L = 0.2 R$; (b) $L = 0.4 R$; (c) $L = 0.6 R$.

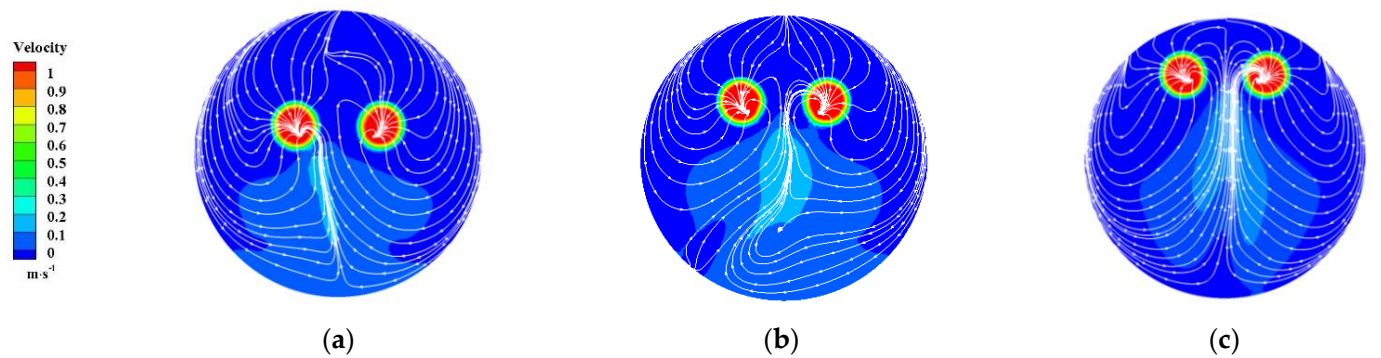


Figure 8. Streamline and velocity distribution nephogram of Section 4-4 under different L values: (a) $L = 0.2 R$; (b) $L = 0.4 R$; (c) $L = 0.6 R$.

3.2. Influence of S on Hydraulic Performance

The inlet condition was kept unchanged, the suspended height was set to $H = 0.6 D$, and the distance between the connecting line of the two pumps and the center of the sump was set to $L = 0.2 R$. The hydraulic performance of prefabricated pumping stations with $S = 0.6 R$, $S = 0.8 R$, and $S = 1.0 R$ was then studied.

Figure 9a shows the curve of the influence of S on the efficiency of the two pumps. According to the curve, the efficiency of Pump I was higher than that of Pump II. The efficiency of Pump I was the highest when $S = 0.8 R$, and the efficiency of Pump II decreased with increasing S .

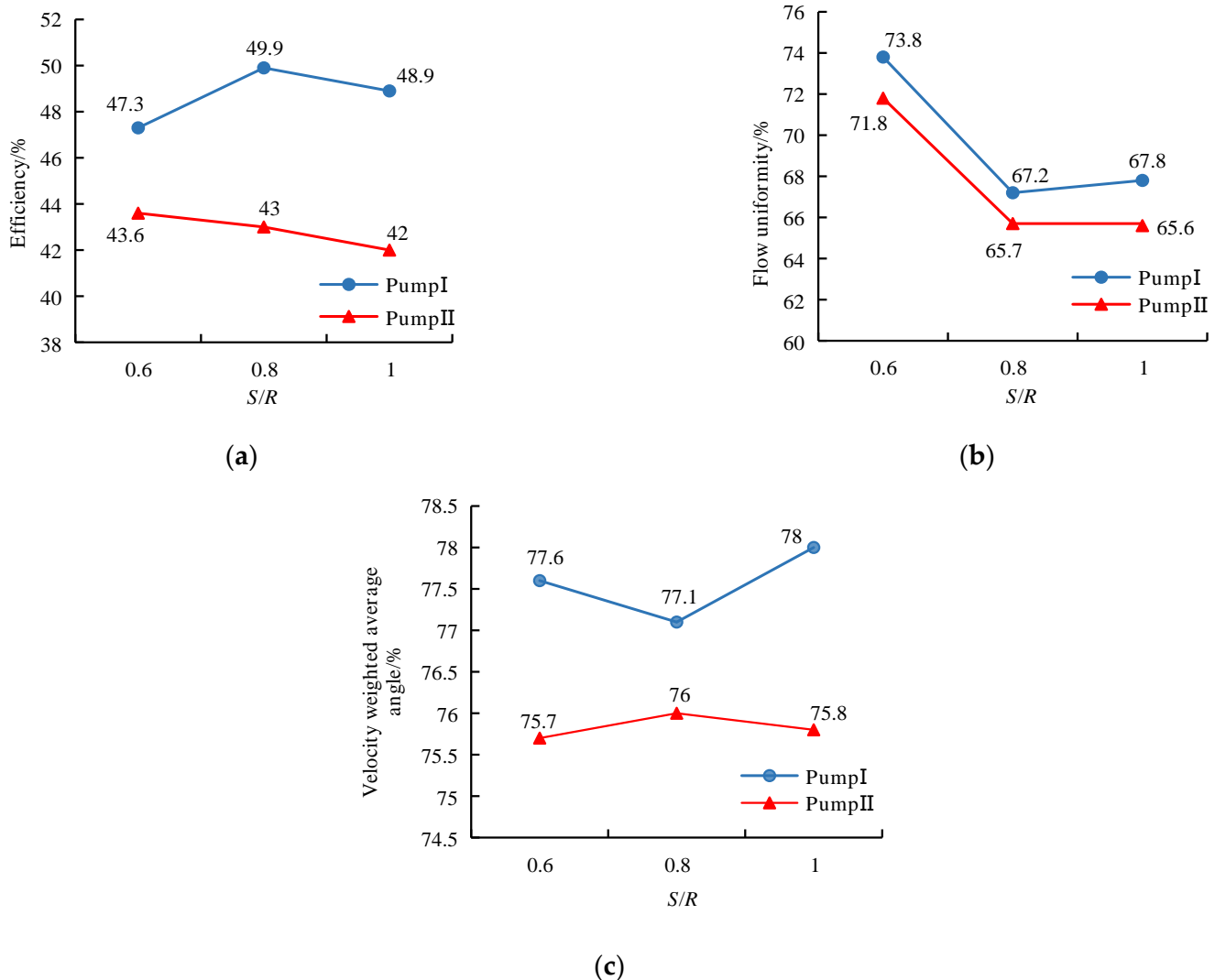


Figure 9. (a) The influence of S on the efficiency of the two pumps; (b) Variation of the inlet velocity uniformity of the pump impeller chamber with S ; (c) The weighted average angle of the inlet velocity of the pump impeller chamber with S .

Figure 9b shows the variation curve of inlet velocity uniformity of the pump impeller chamber with S . It can be seen from the curve that with increasing S , the uniformity of flow velocity at the pump inlet decreased.

Figure 9c shows the curve of the weighted average angle of the inlet velocity of the pump impeller chamber with S . It can be seen from the curve that the influence of S on the weighted average angle of the impeller inlet velocity in Pipe I was greater than that in Pipe II. The weighted average angle of the impeller inlet velocity of Pipe I was higher than that of the impeller inlet of Pipe II under the three schemes.

Figures 10–12 show the streamline and velocity distribution nephograms of sections 1-1, 3-3, and 4-4, respectively, under different S values.

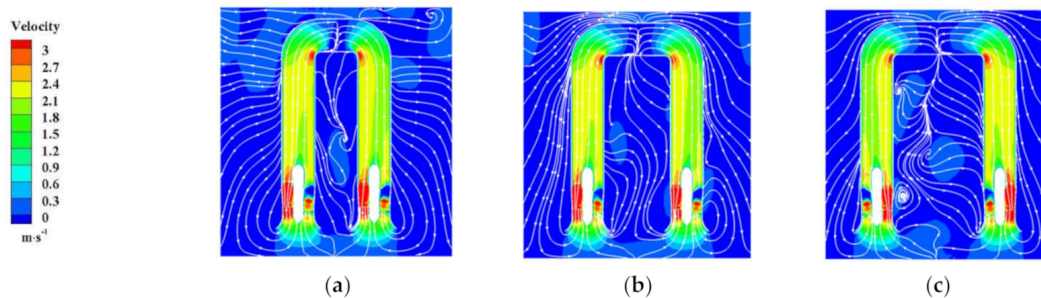


Figure 10. Streamline and velocity distribution nephogram of Section 1-1 under different S values: (a) $S = 0.6 R$; (b) $S = 0.8 R$; (c) $S = 1.0 R$.

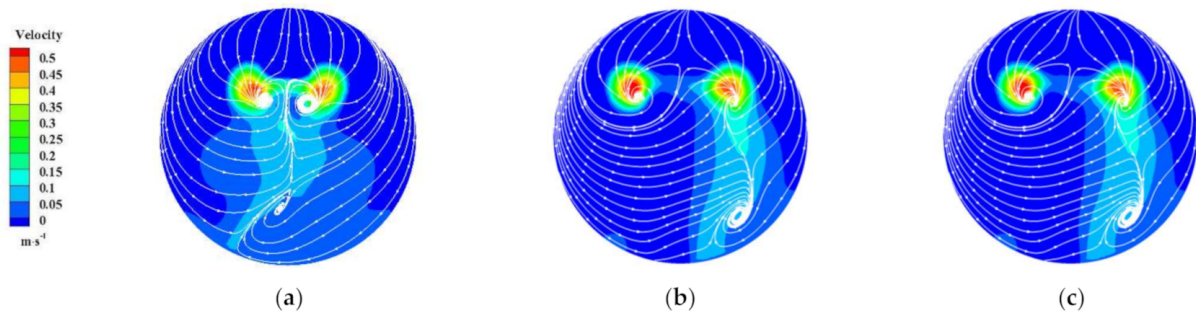


Figure 11. Streamline and velocity nephogram of Section 3-3 of the sump under different S values: (a) $S = 0.6 R$; (b) $S = 0.8 R$; (c) $S = 1.0 R$.

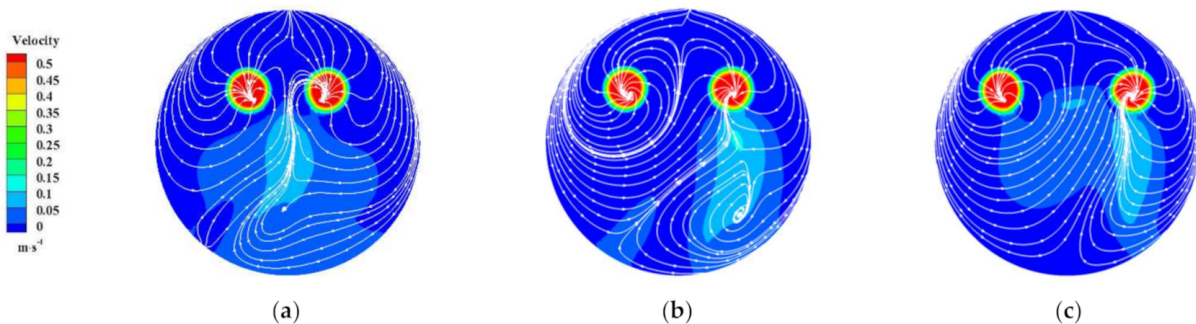


Figure 12. Streamline and velocity nephogram of Section 4-4 of the sump under different S values: (a) $S = 0.6 R$; (b) $S = 0.8 R$; (c) $S = 1.0 R$.

It can be seen from Figure 13 that when $S = 0.6 R$ and $S = 0.8 R$, the streamline distribution was relatively uniform. When the pump spacing S was increased to $1.0 R$, the streamline curvature between the two pipes became slightly more serious, and a vortex appeared near the outlet pipe of Pump II.

It can be seen from Figure 11; Figure 12 that the two swirling currents converged in front of the two pumps. With increasing S , the rotation radius of the streamline increased gradually around the pipe. This made the streamline between the two pipes tend to be uniform and smooth. When $S = 0.6 R$, smaller vortices appeared in the lower area of the suction inlet of the two pumps, but the vortex disappeared at the suction section. At this time, the streamline and velocity distribution were symmetrical. For both $S = 0.8 R$ and $S = 1.0 R$, an obvious vortex appeared in the sump near Pump II. This led to deterioration of the flow

pattern near Pump II, and the efficiency of water Pump II was reduced. The distribution of the side streamline and velocity near the incoming direction was not uniform.

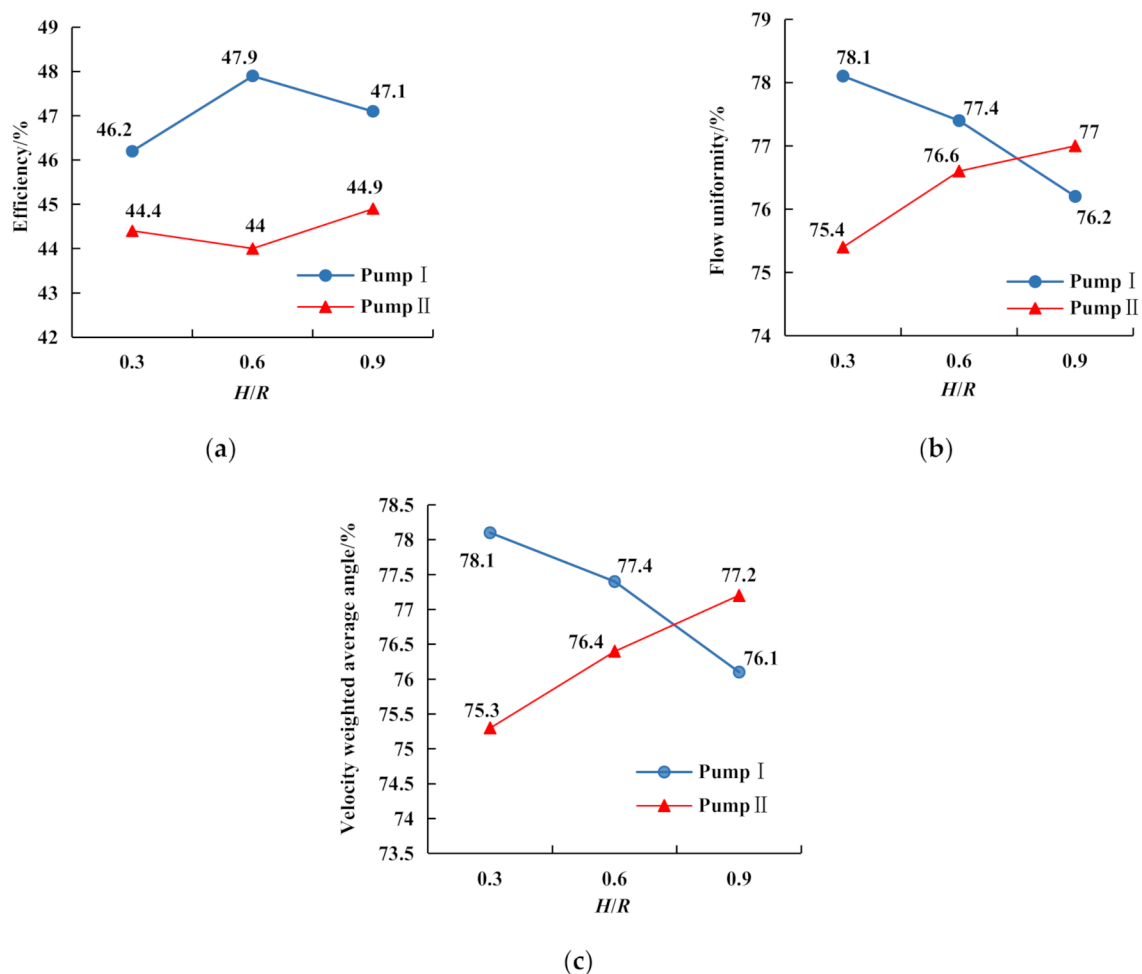


Figure 13. (a) The influence of H on the efficiency of the two pumps; (b) Variation of the inlet velocity uniformity of the pump impeller chamber with H ; (c) The weighted average angle of the inlet velocity of the pump impeller chamber with H .

3.3. Influence of H on Hydraulic Performance

In order to explore the influence of different H values on the hydraulic performance of the prefabricated pumping station, we set the inlet mass flow to $Q = 55 \text{ kg/s}$, the distance between the connecting line of the two pumps and the center of the sump to $L = 0.2 R$, and the distance between the two pumps to $S = 0.6 R$. The respective internal flow characteristics of three schemes with suspended heights of $H = 0.3 D$, $H = 0.6 D$, and $H = 0.9 D$ were then studied.

Figure 13a shows the curve of the influence of H on the efficiency of the two pumps. According to the curve, the efficiency of Pump I was higher than that of Pump II. Moreover, when $H = 0.3\text{--}0.6 D$, the efficiency difference between the two pumps was larger and larger, and the difference was smaller and smaller when $H = 0.6\text{--}0.9 D$.

Figure 13b shows the variation curve of the inlet velocity uniformity of the pump impeller chamber with H . It can be seen from the curve that with increasing suspended height H , the uniformity of the flow velocity at the impeller inlet of Pipe I gradually decreased, while that of Pipe II increased gradually. The two curves intersect at $H = 0.6\text{--}0.9 D$.

Figure 13c shows the curve of the weighted average angle of inlet velocity of the pump impeller chamber with H . It can be seen from the curve that the weighted average angle

of the impeller inlet velocity in Pipe I decreased gradually and that of Pipe II increased gradually.

Figures 14–16 show the streamline and velocity distribution nephograms of sections 1-1, 3-3, and 4-4, respectively, under different H values.

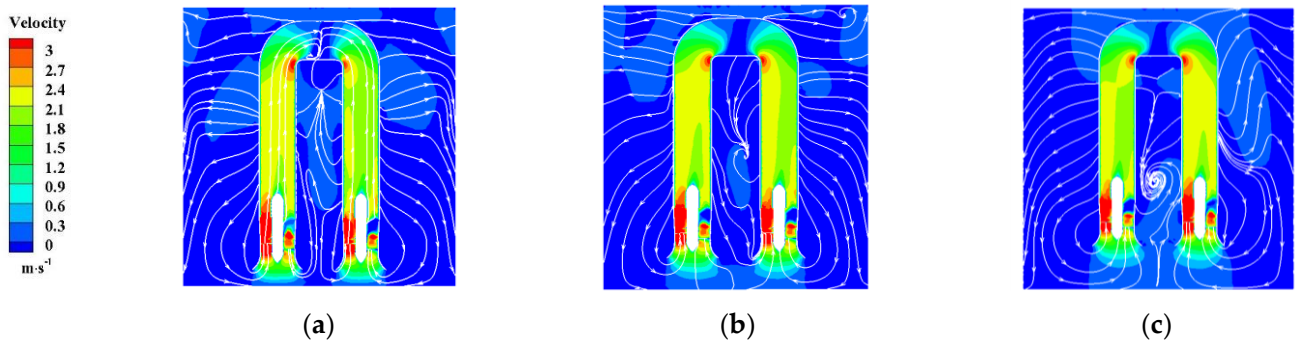


Figure 14. Streamline and velocity distribution nephogram of Section 1-1 under different H values: (a) $H = 0.3 D$; (b) $H = 0.6 D$; (c) $H = 0.9 D$.

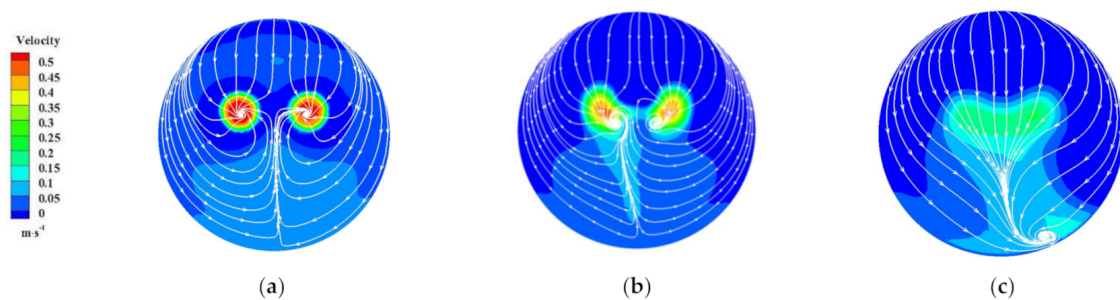


Figure 15. Streamline and velocity nephogram of Section 3-3 of the sump under different H values: (a) $H = 0.3 D$; (b) $H = 0.6 D$; (c) $H = 0.9 D$.

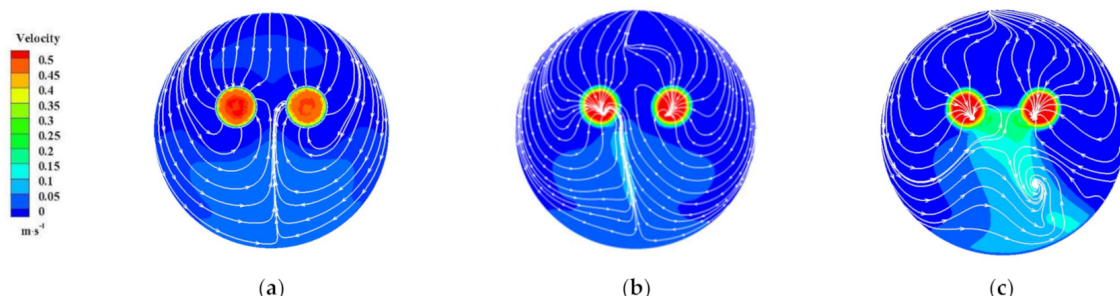


Figure 16. Streamline and velocity nephogram of Section 4-4 of the sump under different H values: (a) $H = 0.3 D$; (b) $H = 0.6 D$; (c) $H = 0.9 D$.

It can be seen from Figure 14 that when the suspended height was changed from $H = 0.3 D$ to $H = 0.9 D$, the streamline curvature became larger and larger, and the degree of uniformity became worse and worse. Specifically, when $H = 0.3 D$, the streamline distribution was more uniform and the velocity distribution was more symmetrical. When $H = 0.6 D$ and $H = 0.9 D$, it can be seen from the streamline diagram of the vertical section that the streamline curvature between the two pipelines changed greatly. A vortex gradually appeared between the two pipes, and the flow pattern was more chaotic.

According to Figure 15; Figure 16, when $H = 0.3 D$, the streamline distribution was more symmetrical, and the velocity distribution was more symmetrical. When $H = 0.6 D$, the flow was no longer symmetrical to the left and right, and the convergence point of the flow shifted. When $H = 0.9 D$, the streamline was symmetrical and the velocity distribution

was uneven. The velocity of water between the front of Pump II and the wall was higher than that of the symmetrical area, and a vortex appeared on the wall in front of Pump II.

4. Conclusions

In the research, CFD numerical simulation was used to explore the influence of L (the distance between the connecting line of two pumps and the center of the sump), S (the distance between the two pumps), and H (the suspension height of the two pumps) on the hydraulic performance of a prefabricated pumping station. It was observed that changes in these geometric parameters had an impact on the internal hydraulic performance of the prefabricated pump station, and the impact on the two symmetrical pumps was not the same.

- (1). In this research, the optimal design parameters for the internal pumps of a prefabricated pump station were determined. When $L = 0.2 R$, $S = 0.6 R$, and $H = 0.6 D$, the hydraulic performance of the prefabricated pump station was better.
- (2). Change in L had little effect on the efficiency of the two pumps, but it had a greater impact on the inlet velocity uniformity and the velocity weighted average angle of the pump impeller chamber. When $L = 0.2 R$, the efficiency of the two pumps was the highest, and the weighted average angle of the impeller chamber inlet velocity was the largest. $L = 0.2 R$ is thus recommended.
- (3). Change in S had little effect on the efficiency of the two pumps, but it had a greater impact on the inlet velocity uniformity and the velocity weighted average angle of the impeller chamber. When $S = 0.6 R$, the velocity uniformity of the impeller chamber inlet was the highest. $S = 0.6 R$ is thus recommended.
- (4). Change in H had little effect on the efficiency of the two pumps, but it had a greater impact on the inlet velocity uniformity and the velocity weighted average angle of the two impeller chambers. When $H = 0.6 D$, the water velocity near the pump inlet was lower, but at $H = 0.9 D$, the inlet velocity of the pump was higher. Considering the discharge of a pumping station, the velocity of the bottom water should reach the starting speed of impurity particles. If the suspended height of the pump is too high, the bottom velocity will be low, which is not conducive to sewage discharge from the prefabricated pump station. $H = 0.6 D$ is thus recommended.

Author Contributions: CFD numerical simulation, B.Z. and M.W.; Data curation, L.C. and C.X.; Writing—original draft, B.Z.; Writing—review and editing, L.C. All authors have read and agreed to the published version of the manuscript

Funding: This research was supported by the National Natural Science Foundation of China (Grant No. 51779214), Peak plan six talents in Jiangsu Province (Grant No. 2015-JXQC-007), Jiangsu Province 333 high-level talents training project, Jiangsu Planned Projects for Postdoctoral Research Funds (Grant No. 1701189B), A Project Funded by the Priority Academic Program Development of Jiangsu Higher Education Institutions (PAPD), and Key Project of Water Resources Technology in Jiangsu Province, China (Grants No. 2019014 and No. 2020027).

Data Availability Statement: The data that support the findings of this study are available from the corresponding author, upon reasonable request.

Conflicts of Interest: The authors declare no conflict of interest.

References

1. Wang, Y. Study on the Designing of the Municipal Underground Wastewater Pumping Station. Master's Thesis, Zhejiang University, Hangzhou, China, 2005.
2. Liu, R.H. Study on Hydraulic Characteristic and Optimum Design of Submerged Pump System. Master's Thesis, Yangzhou University, Yangzhou, China, 2010.
3. Gu, Y.D.; Pei, J.; Yuan, S.Q.; Zhang, J.F. A Pressure Model for Open Rotor–Stator Cavities: An Application to an Adjustable-Speed Centrifugal Pump with Experimental Validation. *J. Fluids Eng.* **2020**, *142*, 101301. [[CrossRef](#)]
4. Jiao, W.; Zhang, D.; Wang, C.; Cheng, L.; Wang, T. Unsteady numerical calculation of oblique submerged jet. *Energies* **2020**, *13*, 4728. [[CrossRef](#)]

5. Zhang, D.; Jiao, W.; Cheng, L.; Xia, C.; Zhang, B.; Luo, C.; Wang, C. Experimental study on the evolution process of the roof-attached vortex of the closed sump. *Renew. Energy* **2021**, *164*, 1029–1038. [[CrossRef](#)]
6. He, X.; Zhang, Y.; Wang, C.; Zhang, C.; Cheng, L.; Chen, K.; Hu, B. Influence of critical wall roughness on the performance of double-channel sewage pump. *Energies* **2020**, *13*, 464. [[CrossRef](#)]
7. Wang, H.; Long, B.; Yang, Y.; Xiao, Y.; Wang, C. Modelling the influence of inlet angle change on the performance of submersible well pumps. *Int. J. Simul. Model.* **2020**, *19*, 100–111. [[CrossRef](#)]
8. Sweeney, C.E.; Elder, R.A.; Hay, D. Pump-Sump Design Experience: Summary. *J. Hydraul. Div.* **1982**, *108*, 361–377. [[CrossRef](#)]
9. Iversen, H. Studies of submergence requirements of high-specific-speed pumps. *Trans. ASME* **1953**, *75*, 635.
10. Sakai, H. Pumping Station Engineering Handbook. *Jpn. Assoc. Agric. Eng. Enterp. Tokyo* **1991**, *1*, 304–307.
11. Fraser, W. Hydraulic problems encountered in intake structures of vertical wet-pit pumps and methods leading to their solution. *Trans. ASME* **1953**, *75*, 643–652.
12. Ansar, M.; Nakato, T. Experimental study of 3D pump-intake flows with and without cross flow. *J. Hydraul. Eng.* **2001**, *127*, 825–834. [[CrossRef](#)]
13. Liu, Q.; Kang, C.; Li, M. Flow Features of a Prefabricated Pumping Station Operating under High Flow Rate Conditions. *Int. J. Fluid Mach. Syst.* **2018**, *11*, 171–180. [[CrossRef](#)]
14. Wang, K.; Hu, J.; Liu, H.; Zhang, Z.; Zou, L.; Lu, Z. Research on the Deposition Characteristics of Integrated Prefabricated Pumping Station. *Symmetry* **2020**, *12*, 760. [[CrossRef](#)]
15. Li, Q.; Kang, C.; Teng, S.; Li, M. Optimization of Tank Bottom Shape for Improving the Anti-Deposition Performance of a Prefabricated Pumping Station. *Water* **2019**, *11*, 602. [[CrossRef](#)]
16. Medina, A.P. Design of a prefabricated station for collecting, separating and pumping in a closed cycle. *Ing. Pet. (Mex.)* **1972**, *12*, 18–22.
17. Hu, K.; Zhou, Y.; Chen, J. Optimal design of effective capacity of intergrated prefabricated pumping station. *Gen. Mach.* **2016**, *3*, 7–79.
18. Hu, K. Self-cleaning of integrated prefabricated pumping station. *Gen. Mach.* **2019**, *11*, 15–17.
19. Cheng, L.; Zhou, J.R.; Wang, M.; Che, X.H.; Xia, C.Z. A Self-Cleaning Method for the Bottom of Prefabricated Pumping Station. CN105002980A, 28 October 2015.
20. Silva, J.M.; Li, S. Numerical simulation of flow in practical water-pump intakes. In *Proceedings of the XXIX IAHR Congress, Beijing, China, 16–21 September 2001*; IAHR: Madrid, Spain, 2001; Volume 9.
21. Li, S.; Lai, Y.; Weber, L.; Silva, J.M.; Patel, V.C. Validation of a three-dimensional numerical model for water-pump intakes. *J. Hydraul. Res.* **2004**, *42*, 282–292. [[CrossRef](#)]
22. Yan, C. New computational methods for fluid flow (1). *Fluid Mach.* **1994**, *8*, 35–38.
23. Yan, C. New computational methods for fluid flow (2). *Fluid Mach.* **1994**, *9*, 33–37.
24. Karassik, I.J.; Messina, J.P.; Cooper, P.; Heald, C.C. *Pump Handbook*; McGraw-Hill Professional Publishing: New York, NY, USA, 2001.
25. Hydraulic Institute. *American National Standard for Pump Intake Design*; ANSI: New York, NY, USA, 1998.
26. Liu, C. *Pump and Pumping Station*; China Water and Power Press: Beijing, China, 2008.
27. Wang, Z.Y.; Wu, E.C.; Guo, D.R. Optimization of prefabricated pumping station in the application of small and medium sized pumping stations. In *Proceedings of the 7th International Symposium on Urban Water Development, Ningbo, China, 11–12 May 2012*; Volume 10.
28. Zhang, J.L.; Lu, Z.L. Discussion on selection and application of drainage pumping station type. *China Water Wastewater* **2016**, *32*, 38–40.
29. Launder, B.E.; Spalding, D.B. *Lectures in Mathematical Models of Turbulence*; Academic Press: Waltham, MA, USA, 1972.
30. Shih, T.H.; Liou, W.W.; Shabbir, A.; Yang, Z.; Zhu, J. A new $k-\epsilon$ eddy viscosity model for high Reynolds number turbulent flows. *Comput. Fluids* **1995**, *24*, 227–238. [[CrossRef](#)]